Responses of Airport Runway Lighting System to Direct Lightning Strikes: Comparisons of TLM Predictions With Experimental Data

Nelson Theethayi, *Member, IEEE*, Vladimir A. Rakov, *Fellow, IEEE*, and Rajeev Thottappillil, *Senior Member, IEEE*

***Abstract*—A test airport runway lighting system, including a buried cable protected by a counterpoise and vertical ground rods, was subjected to direct lightning strikes, and currents and voltages measured in different parts of the system were reported earlier by Bejleri *et al.* In this paper, we attempt to model the lightning interaction with this system using the transmission line theory. Lumped devices along the cable such as current regulator and transformers are ignored; possible nonlinear phenomena (arcing) in the system are neglected; the soil is assumed to be homogeneous. The model-predicted currents in the counterpoise, ground rod, and the cable are compared with the measurements, and a reasonable agreement was found for the currents along the counterpoise. It is found that current in the counterpoise is not much influenced by the presence of the cable. Further, vertical ground rods connected to the counterpoise do not have significant influence on the current distribution along the counterpoise. It appears that the model is unable to predict cable currents and voltages in the test system, presumably due to neglecting nonlinear phenomena in the soil and in cable's insulation and electromagnetic coupling with the lightning channel.**

***Index Terms*—Buried cables, counterpoise, lightning, lighting system, transient analysis, transmission line modeling (TLM).**

I. Introduction

LIGHTNING strikes can cause damage to airport runway lighting systems. In order to better understand the mechanism of lightning interaction with such systems and to access the efficacy of their lightning protection employed by the U.S. Federal Aviation Administration, Bejleri *et al.* [1] conducted an experimental study of the test airport runway system. In their experiments conducted at Camp Blanding, Florida, lightning was triggered using the rocket-and-wire technique. This study is an attempt to simulate the experiments of Bejleri *et al.* [1] using a model based on the transmission line theory [3]–[7]. Sensitivity analysis is performed to identify the factors that influence model predictions.

Manuscript received November 8, 2007; revised March 3, 2008. This work was supported in part by the Swedish Research Council under VR Grant 621-2005-5939, in part by B. John F. and Svea Andersson donation fund, and in part by the National Science Foundation under Grant ATM-0346164.

N. Theethayi and R. Thottappillil are with the Division for Electricity, Department of Engineering Sciences, Uppsala University, S-75121 Uppsala, Sweden (e-mail: nelson.theethayi@angstrom.uu.se; rajeev.thottappillil@angstrom.uu.se).

V. A. Rakov is with the Department of Electrical and Computer Engineering, University of Florida, Gainesville, FL 32611-6130 USA, and also with the International Center for Lightning Research and Testing, Starke, FL 32091 USA (e-mail: rakov@ece.ufl.edu).

Color versions of one or more of the figures in this paper are available online at http://ieeexplore.ieee.org.

Digital Object Identifier 10.1109/TEMC.2008.926907

Under direct lightning strike conditions, insulation breakdown and/or soil ionization can occur in the buried lighting system (involving both insulated and bare conductors). Weather conditions and ground inhomogeneities introduce uncertainties in values of ground conductivity and ground permittivity. Further, there are some lumped elements, including a current regulator, transformers, can- and stake-mounted lights, etc., whose characteristics required for lightning interaction modeling are not available. Finally, there are limitations and uncertainties associated with the measurements. All these factors are disregarded in our initial modeling attempt presented in this paper.

II. Runway Lighting System Tested by Bejleri *et al.*

The test airport runway system tested by Bejleri *et al.* was similar to those found in many small airports. The schematic representation of this test runway and its lighting system, which still exists at the International Center for Lightning Research and Testing (ICLRT) at Camp Blanding, Florida, can be found in [1] and [2]. Different configurations were tested. Only one configuration (configuration 4) is considered here.

Schematic representation of the system for configuration 4 is shown in Fig. 1. The runway pavement is about 92 m $\times$ 23 m. The lighting system includes a generator, current regulator, both placed in the electrical vault, and a buried series lighting cable (outer radius of about 5 mm and central conductor radius being 1.6 mm) feeding, via insulating transformers, five equally spaced stake-mounted lights (cable directly buried in the soil and note that in the experiments corresponding to configuration 4 by Bejleri *et al.* [1], one of the stake-mounted lights was removed as shown in Fig. 1) and five equally spaced can-mounted lights [cable placed in a buried polyvinyl chloride (PVC) pipe of 2.5 cm radius and about 4-mm thick] on either side of the runway, and two signs at the corners (northeast and southwest) of the runway. The insulated single-conductor unshielded cable is buried at a depth of 0.4 and 3 m away from the pavement edge. A counterpoise, a bare copper wire of diameter 4.11 mm, is placed about 10 cm directly above the cable. When the lightning current enters the ground, the counterpoise is expected to intercept the current thereby protecting the cable from direct current injection. The counterpoise is connected to three vertical ground rods, as shown in Fig. 1, which have a length of 2.4 m and 1.56 cm diameter, as well as to all the stakes and cans. The later connections are not shown in Fig. 1. As shown in Fig. 1, currents along the cable and the counterpoise and in the ground rods were measured (a total of 11 current measurements), when the lightning current was injected into the counterpoise.

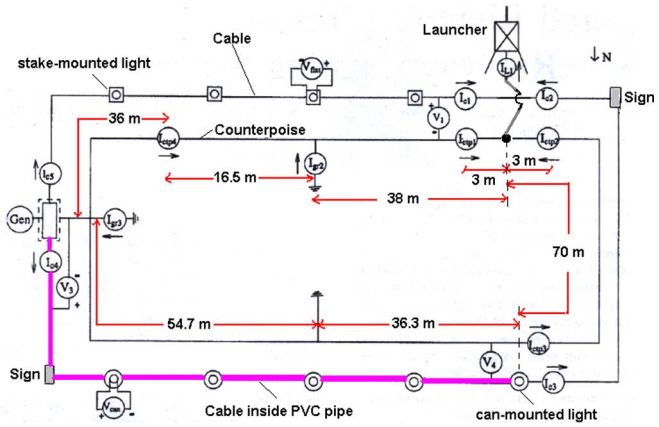

Fig. 1. Measurement points along the cable and counterpoise for configuration 4 [1], [2].

Voltages have also been measured at five points, as shown in Fig. 1. We will compare predictions of the model presented in this paper with the experimental results for the configuration shown in Fig. 1.

III. Transmission Line Model of the System

In case of direct current injection into the counterpoise, current waves propagate along the counterpoise and, depending upon the conductivity of the soil, some current leaks into the ground. There will also be induced currents in the cable due to the electromagnetic coupling between the cable and counterpoise. We shall describe the propagation of current pulses in the test system based on the multiconductor transmission line (MTL) theory.

The coupled transmission line equations for the counterpoise and the cable are given in the frequency domain by the voltage (1) and current (2) wave equations, for an arbitrary propagation direction, say, x. Note that the counterpoise and the cable each form a buried horizontal loop (discussed later), with the counterpoise loop being above the cable loop.

$$\begin{bmatrix} \dfrac{dV_{\rm cab}\,(x,j\omega)}{dx} \\ \dfrac{dV_{\rm cnt}\,(x,j\omega)}{dx} \end{bmatrix} + [Z] \begin{bmatrix} I_{\rm cab}\,(x,j\omega) \\ I_{\rm cnt}\,(x,j\omega) \end{bmatrix} = \begin{bmatrix} 0 \\ 0 \end{bmatrix} \tag{1}$$

$$\begin{bmatrix} \dfrac{dI_{\rm cab}\,(x,j\omega)}{dx} \\ \dfrac{dI_{\rm cnt}\,(x,j\omega)}{dx} \end{bmatrix} + [Y] \begin{bmatrix} V_{\rm cab}\,(x,j\omega) \\ V_{\rm cnt}\,(x,j\omega) \end{bmatrix} = \begin{bmatrix} 0 \\ 0 \end{bmatrix}. \tag{2}$$

In (1) and (2), $V_{\rm cnt}(x,j\omega)$ and $I_{\rm cnt}(x,j\omega)$ are the voltage and current at point x along the counterpoise, respectively, and $V_{\rm cab}(x,j\omega)$ and $I_{\rm cab}(x,j\omega)$ are the voltage and current at point x along the cable, respectively. In (1), $[Z]$ is the per unit length series impedance matrix whose elements are self-impedances of the counterpoise and cable and the mutual impedance between them. In (2), $[Y]$ is the per unit length shunt admittance matrix whose elements are self-admittances of the counterpoise and cable and the mutual admittance between them. For a given source, the magnitude and shape of the voltage or current pulses propagating along the cable and counterpoise are largely determined by the impedance and admittance values. Those values are dependent on the geometry (wire radii, conductor separation, and burial depths) ground conductivity, ground permittivity, and properties of insulation material. We use here the transmission line model (TLM) for buried conductors described in [3], [6], and [7]. Elements of 2×2 symmetric impedance matrix Z in (1) are given by

$$Z_{11} = \left[\begin{array}{l} \dfrac{\sqrt{j\omega\mu_2\sigma_2}}{2\pi\sigma_2 R_c} \dfrac{I_0\left(R_c\sqrt{j\omega\mu_2\sigma_2}\right)}{I_1\left(R_c\sqrt{j\omega\mu_2\sigma_2}\right)} + \dfrac{j\omega\mu_0}{2\pi} \ln\left(\dfrac{R_X}{R_c}\right) \\ \quad + \dfrac{j\omega\mu_0}{2\pi} \left\{ \ln\left(\dfrac{1+\gamma_g R_X}{\gamma_g R_2}\right) + \dfrac{2e^{-2d_2|\gamma_g|}}{4+R_X^2\gamma_g^2} \right\} \end{array} \right] \tag{3a}$$

$$Z_{22} = \left[\begin{array}{l} \dfrac{\sqrt{j\omega\mu_1\sigma_1}}{2\pi\sigma_1 R_1} \dfrac{I_0\left(R_1\sqrt{j\omega\mu_1\sigma_1}\right)}{I_1\left(R_1\sqrt{j\omega\mu_1\sigma_1}\right)} \\ \quad + \dfrac{j\omega\mu_0}{2\pi} \left\{ \ln\left(\dfrac{1+\gamma_g R_1}{\gamma_g R_1}\right) + \dfrac{2e^{-2d_1|\gamma_g|}}{4+R_1^2\gamma_g^2} \right\} \end{array} \right] \tag{3b}$$

$$Z_{12} = Z_{21} = \frac{j\omega\mu_0}{2\pi} \left\{ \ln\left(\frac{1+\gamma_g D}{\gamma_g D}\right) + \frac{2e^{-(d_1+d_2)|\gamma_g|}}{4+D^2\gamma_g^2} \right\} \tag{3c}$$

where $\gamma_g = \sqrt{j\omega\mu_0\,(\sigma_g + j\omega\varepsilon_g)}$. In the previous equations, R_c, R_1, d_1, d_2, and D are the inner (conductor) radius of the cable, the radius of the counterpoise, depth of counterpoise, depth of cable, and vertical separation between the cable and the counterpoise, respectively. $I_0(\cdot)$ and $I_1(\cdot)$ are Bessel's functions of first kind with order zero and one, respectively. In (3b), $R_X = R_2$ the outer radius of the cable for the cable section in direct contact with the soil, and $R_X = R_p$ (the outer radius of the PVC pipe) for the section that is placed in buried PVC pipe. In (3), μ_0 is the free-space permeability and σ_g and ε_g are the ground conductivity and permittivity, respectively. Also, in (3), μ_1 and σ_1 are the permeability and conductivity of the counterpoise material and μ_2 and σ_2 are the permeability and conductivity of the cable conductor material.

Elements of 2×2 symmetric admittance matrix Y in (2) are given by

$$Y_{11} = y_{g22} + \frac{y_{g12}(y_{g11} + j\omega C_{\rm eff})}{j\omega C_{\rm eff} + y_{g11} + y_{g12}} \tag{4a}$$

$$Y_{22} = \frac{j\omega C_{\rm eff}\,(y_{g11} + y_{g12})}{j\omega C_{\rm eff} + y_{g11} + y_{g12}} \tag{4b}$$

$$Y_{12} = -\frac{j\omega C_{\rm eff}\, y_{g12}}{j\omega C_{\rm eff} + y_{g11} + y_{g12}} \tag{4c}$$

where

$$\begin{bmatrix} y_{g11} & y_{g12} \\ y_{g21} & y_{g22} \end{bmatrix} = \begin{bmatrix} Y_{11} + Y_{12} & -Y_{g12} \\ -Y_{12} & Y_{g22} + Y_{g12} \end{bmatrix} \tag{5}$$

$$\begin{bmatrix} Y_{g11} & Y_{g12} \\ Y_{g21} & Y_{g22} \end{bmatrix} \approx \gamma_g^2 \begin{bmatrix} Z_{g11} & Z_{g12} \\ Z_{g21} & Z_{g22} \end{bmatrix}^{-1}. \tag{6}$$

In (6), the matrix Z_g is the matrix of ground impedance whose elements are given by (3) with terms involving γ_g only. Note that in (4), $C_{\rm eff}$ is the effective capacitance depending upon

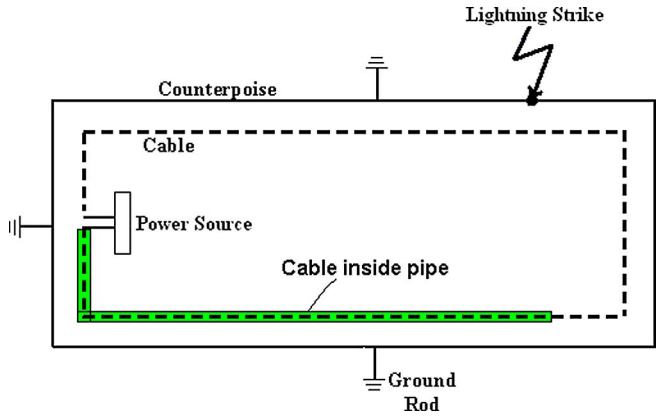

Fig. 2. Schematic representation of the modeled distributed-circuit system containing buried counterpoise (solid line) and cable (dashed line).

whether the section of cable is in contact with the soil or placed in a buried pipe. If the cable is in contact with the soil, then $C_{\text{eff}} = 2\pi\varepsilon_1[\ln(R_2/R_c)]^{-1}$, where ε_1 is the permittivity of the cable insulation. For the cable section in the PVC pipe, C_{eff} is C_P as given by

$$C_P = \left[\frac{1}{C_i} + \frac{1}{C_a} + \frac{1}{C_w}\right]^{-1} \tag{7a}$$

$$C_i = 2\pi\varepsilon_1 \left[\ln\left(\frac{R_2}{R_c}\right)\right]^{-1} \tag{7b}$$

$$C_a = 2\pi\varepsilon_0 \left[\ln\left(\frac{R_p - t_w}{R_2}\right)\right]^{-1} \tag{7c}$$

$$C_w = 2\pi\varepsilon_2 \left[\ln\left(\frac{R_p}{R_p - t_w}\right)\right]^{-1} \tag{7d}$$

and is the series combination of the capacitance due to cable insulation, that due to the air insulation between cable and the inner surface of the PVC pipe and that due to the PVC pipe wall. In (7), ε_0 and ε_2 is the free-space permittivity and the permittivity of the PVC pipe, respectively, and t_w is the PVC pipe wall thickness.

IV. Application of the Model to Configuration Shown in Fig. 1

A schematic representation of the system under study is shown in Fig. 2. Lightning strike is represented by a lumped current source. There should be electromagnetic coupling between the lightning channel located above the injection point and buried conductors, but it is not included in the simulations presented here. As stated in Section I, nonlinear processes such as breakdown between cable and counterpoise and soil ionization around the counterpoise, if any, are neglected.

For the simulations, we use the measured return stroke current I_{L1} corresponding to stroke 1 of Flash U9841 presented by Bejleri *et al.* [1], [2] whose waveform we approximated by $I_{L1}(t) = 16 \times 10^3(e^{-8.5\times10^3 t} - e^{-2.0\times10^6 t})$ (see Fig. 3), where I_{L1} is in amperes and t is in seconds. The total length of

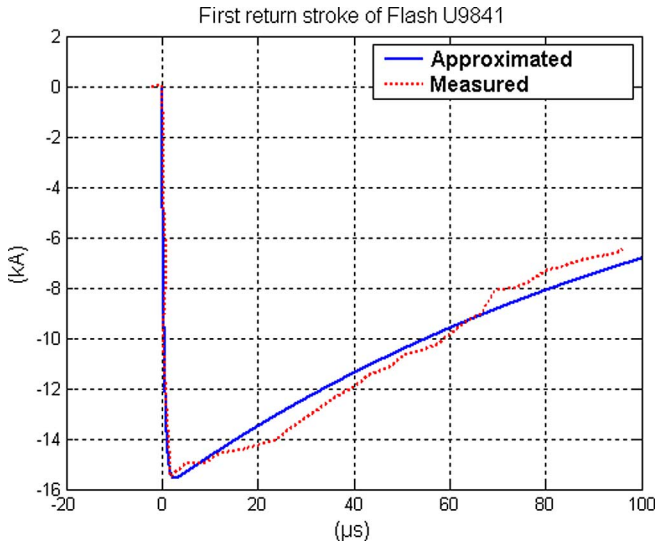

Fig. 3. Measured and approximated total lightning currents.

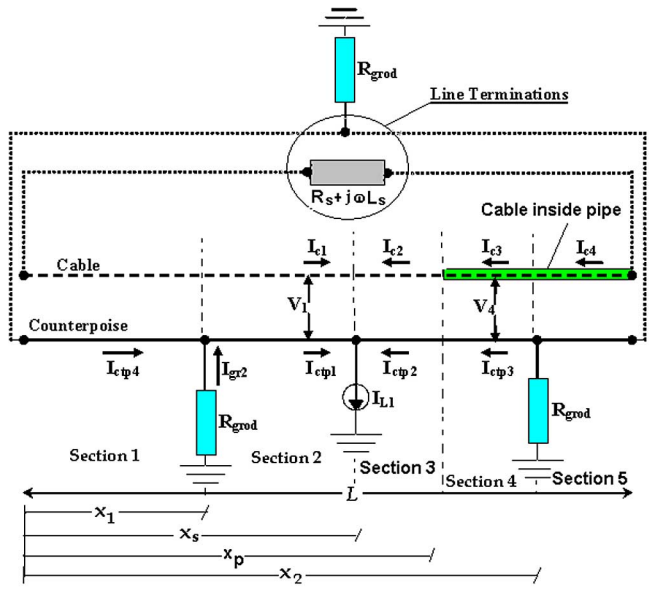

Fig. 4. Diagram showing section boundary conditions on the transmission line and the measurement points for currents on the counterpoise (solid line and with current subscripts "ctp") and the cable (dashed line and with current subscripts "c"), as well as for voltages between the cable and counterpoise. Distances are not to scale. Also shown is the section of cable inside the pipe. Dotted lines connecting the line ends to their terminations represent short circuits. Line terminations are at the electric vault.

each of the two loop conductors is about 251.5 m and, as per Fig. 4, if traversed from left to right, the ground rods are located at 0 m (termination), 52.5 m (x_1), and 196.8 m (x_2). The lightning current injection point is located at 90.5 m (x_s). The cable section inside the pipe begins at 160.5 m (x_p). The sensors measuring currents and voltages are located at approximate distances from the current injection point that are given in Table I.

The presence of insulating transformers along the cable is neglected and the source (generator and current regulator) is replaced by a 2-Ω series resistor (R_s) and a series inductor of

TABLE I
MEASUREMENT POINT LOCATIONS

Measurement point label	Description	Distance from current injection point (m)
I_{L1}	Injected lightning current	0
I_{ctp1}	Current in the counterpoise in Section 2	3
I_{ctp2}	Current in the counterpoise in Section 3	3
I_{ctp3}	Current in the counterpoise in Section 3	70
I_{ctp4}	Current in the counterpoise in Section 1	54.5
I_{c1}	Current in the cable in Section 2	3
I_{c2}	Current in the cable in Section 3	3
I_{c3}	Current in the cable in Section 3	70
I_{c4}	Current in the cable in Section 4	161
I_{gr2}	Current into ground rod at the junction of Sections 1 and 2	38
V_1	Voltage between cable and counterpoise in Section 2	3
V_4	Voltage between cable and counterpoise in Section 3	70

1 mH (L_s). The values of resistance and inductance are expected ball-park values. The ground rods are modeled as lumped shunt resistances at the appropriate locations along the counterpoise. The resistance of the ground rod is calculated using [4], [5], [8]

$$R_{\mathrm{grod}} = \frac{1}{2\pi\sigma_g l_{\mathrm{rod}}}\left[\ln\left(\frac{4l_{\mathrm{rod}}}{a_{\mathrm{rod}}}\right) - 1\right]. \tag{8}$$

In (8), l_{rod} is the length of the rod (around 2.4 m) and a_{rod} is the radius of the rod (about 0.78 cm). The shunt resistance representation of the ground rod is adopted under the assumptions that $l_{\mathrm{rod}} \ll \sqrt{2/\omega\mu_0\sigma_g}$ and $l_{\mathrm{rod}} \gg a_{\mathrm{rod}}$, which is valid for the system under study.

In general, the solution for voltages and currents in any MTL system can be obtained by the modal analysis. This involves decoupling of the transmission line (TL) equations (1) and (2) and solving for either the modal currents or modal voltages with appropriate section boundary conditions. The actual currents and voltages are related to the modal currents and voltages through the transformation matrix [5]. This procedure for TL equations used in the present study is as follows. Let us divide the MTL into five sections, marked in Fig. 4. The solutions for the voltage and current are given by [5]

$$V(x) = Z_c T\left(e^{-\gamma x} I^{+}_{\mathrm{ms}} + e^{\gamma x} I^{-}_{\mathrm{ms}}\right) \tag{9a}$$

$$I(x) = T\left(e^{-\gamma x} I^{+}_{\mathrm{ms}} - e^{\gamma x} I^{-}_{\mathrm{ms}}\right). \tag{9b}$$

In (9), T is the transformation matrix that depends on the eigenvalues of the product of impedance and admittance matrices of the transmission line (appropriate product of impedance and admittance depending on the section of the cable in soil or in the pipe), the subscript "s" represents section number, and γ and Z_c are given by (10) and (11), respectively

$$\gamma = \sqrt{T^{-1}YZT} \tag{10}$$

$$Z_c = ZT\gamma^{-1}T^{-1} \tag{11}$$

$$\left\{\begin{array}{l} Z_c' T' e^{-\gamma' x_1} I^{+}_{m2} + Z_c' T' e^{\gamma' x_1} I^{-}_{m2} \\ \quad -Z_c' T' e^{-\gamma' x_1} I^{+}_{m1} - Z_c' T' e^{\gamma' x_1} I^{-}_{m1} \end{array}\right\} = 0 \tag{12a}$$

$$\left\{\begin{array}{l} T' e^{-\gamma' x_1} I^{+}_{m1} - T' e^{\gamma' x_1} I^{-}_{m1} \\ \quad + \left(-T' + Z_c' T' G_s\right) e^{-\gamma' x_1} I^{+}_{m2} \\ \quad + \left(T' + Z_c' T' G_s\right) e^{\gamma' x_1} I^{-}_{m2} \end{array}\right\} = 0. \tag{12b}$$

Similarly, at distance $x = x_s$ (see Fig. 4)

$$\left\{\begin{array}{l} Z_c' T' e^{-\gamma' x_s} I^{+}_{m3} + Z_c' T' e^{\gamma' x_s} I^{-}_{m3} \\ \quad -Z_c' T' e^{-\gamma' x_s} I^{+}_{m2} - Z_c' T' e^{\gamma' x_s} I^{-}_{m2} \end{array}\right\} = 0 \tag{13a}$$

$$\left\{\begin{array}{l} T' e^{-\gamma' x_s} I^{+}_{m3} - T' e^{\gamma' x_s} I^{-}_{m3} \\ \quad -T' e^{-\gamma' x_s} I^{+}_{m2} + T' e^{\gamma' x_s} I^{-}_{m2} \end{array}\right\} = I_0. \tag{13b}$$

Similarly, at distance $x = x_p$ (see Fig. 4)

$$\left\{\begin{array}{l} Z_c'' T'' e^{-\gamma'' x_p} I^{+}_{m4} + Z_c'' T'' e^{\gamma'' x_p} I^{-}_{m4} \\ \quad -Z_c' T' e^{-\gamma' x_p} I^{+}_{m3} - Z_c' T' e^{\gamma' x_p} I^{-}_{m3} \end{array}\right\} = 0 \tag{14a}$$

$$\left\{\begin{array}{l} T'' e^{-\gamma'' x_p} I^{+}_{m4} - T'' e^{\gamma'' x_p} I^{-}_{m4} \\ \quad -T' e^{-\gamma' x_p} I^{+}_{m3} + T' e^{\gamma' x_p} I^{-}_{m3} \end{array}\right\} = 0. \tag{14b}$$

At distance $x = x_2$ (see Fig. 4)

$$\left\{\begin{array}{l} Z_c'' T'' e^{-\gamma'' x_2} I^{+}_{m5} + Z_c'' T'' e^{\gamma'' x_2} I^{-}_{m5} \\ \quad -Z_c'' T'' e^{-\gamma'' x_2} I^{+}_{m4} - Z_c'' T'' e^{\gamma'' x_2} I^{-}_{m4} \end{array}\right\} = 0 \tag{15a}$$

$$\left\{\begin{array}{l} T'' e^{-\gamma'' x_2} I^{+}_{m4} - T'' e^{\gamma'' x_2} I^{-}_{m4} \\ \quad + \left(-T'' + Z_c'' T'' G_s\right) e^{-\gamma'' x_2} I^{+}_{m5} \\ \quad + \left(T'' + Z_c'' T'' G_s\right) e^{\gamma'' x_2} I^{-}_{m5} \end{array}\right\} = 0 \tag{15b}$$

$$G_s = \begin{bmatrix} 0 & 0 \\ 0 & 1/R_{\mathrm{grod}} \end{bmatrix}. \tag{16}$$

We can use the previous equations and appropriate section boundary conditions to write the following set of linear simultaneous equations for each section. For convenience, let us assume that T', Z_c', γ' are the transformation matrix, characteristic impedance, and propagation constant, respectively, for the MTL section where the cable is in the soil and T'', Z_c'', γ'' are the corresponding terms for the MTL section where the cable is in the pipe. At distance $x = x_1$ (see Fig. 4), the voltage is continuous and current is discontinuous due to the presence of ground rod.

At distances $x = 0$ and $x = L$, the node equations are (17) and (18), respectively

$$\left\{\begin{array}{l} Z_c' T' \left(G_{11} + G_{12}\right) I^{+}_{m1} + Z_c' T' \left(G_{11} + G_{12}\right) I^{-}_{m1} \\ \quad -Z_c'' T'' G_{12} e^{-\gamma'' L} I^{+}_{m5} - Z_c'' T'' G_{12} e^{\gamma'' L} I^{-}_{m5} \\ \quad -T' I^{+}_{m1} + T' I^{-}_{m1} \end{array}\right\} = 0 \tag{17}$$

$$\left\{\begin{array}{l} -Z_c' T' G_{12} I_{m1}^{+} - Z_c' T' G_{12} I_{m1}^{-} + T'' e^{-\gamma'' L} I_{m5}^{+} \\ \quad + Z_c'' T'' \left(G_{11} + G_{12}\right) e^{-\gamma'' L} I_{m5}^{+} \\ \quad + Z_c'' T'' \left(G_{11} + G_{12}\right) e^{-\gamma'' L} I_{m5}^{-} - T'' e^{-\gamma'' L} I_{m5}^{-} \end{array}\right\} = 0 \tag{18}$$

$$G_{11} = \begin{bmatrix} 0 & 0 \\ 0 & 1/(2R_{\mathrm{grod}}) \end{bmatrix} \tag{19}$$

$$G_{12} = \begin{bmatrix} (R_s + j\omega L)^{-1} & 0 \\ 0 & 1 \times 10^{6} \end{bmatrix}. \tag{20}$$

Solution of the previous linear simultaneous equations gives us I_{ms}^{+} and I_{ms}^{-} corresponding to a given section, which can be used in (9) to get the current and voltage at any point on the conductor. Next, we present results of simulations, comparison with measurements, and sensitivity analysis.

V. Results

There is an uncertainty regarding ground conductivity at Camp Blanding, but it is probably between 1 mS/m (resistivity 1000 Ω m) and 0.25 mS/m (resistivity 4000 Ω m) [1]. For this reason, we will show simulation results corresponding to two values of ground conductivity 1 and 0.25 mS/m. The ground relative permittivity was assumed to be 10. In each of the figures showing model predicted waveforms corresponding measured waveforms are presented as well.

A. Counterpoise and Ground Rod Currents—Single Conductor With Ground Return Analysis

In this section, we will first examine influence of the cable on currents in the counterpoise by neglecting the cable and comparing model predictions with the corresponding measurements. Further, in order to evaluate the efficacy of the three ground rods, we will consider cases with and without ground rods. A model for a single buried bare wire is found in [6]. Fig. 5 shows currents I_{ctp1} (first window), I_{ctp2} (second window), I_{ctp3} (third window), and I_{ctp4} (fourth window), and Fig. 6 shows the ground rod currents I_{gr2}.

It seems that the presence of ground rods does not have any significant influence on the current distribution along the counterpoise. This observation holds for either of the two ground conductivity values considered. It is also important to note that the current distribution along the counterpoise is relatively insensitive to ground conductivity. As expected, close to the current injection point, counterpoise currents I_{ctp1} and I_{ctp2} (see Fig. 5, first and second windows) are least affected by changes in ground conductivity. Farther from the injection point, effects of ground conductivity are more appreciable, particularly in terms of current rise time (see Fig. 5, third and fourth windows). The simulated current peaks into the ground rod I_{gr2} (see Fig. 6) are somewhat larger than the measured current peak, particularly for the case of 1 mS/m ground conductivity.

The simulations show that I_{ctp1} is less than I_{ctp2}, but the measurements show otherwise. Further, measurements show an unusual waveshape (the tail decaying to zero at about 30 μs) for I_{ctp3}, while the corresponding simulations predict a very dif-

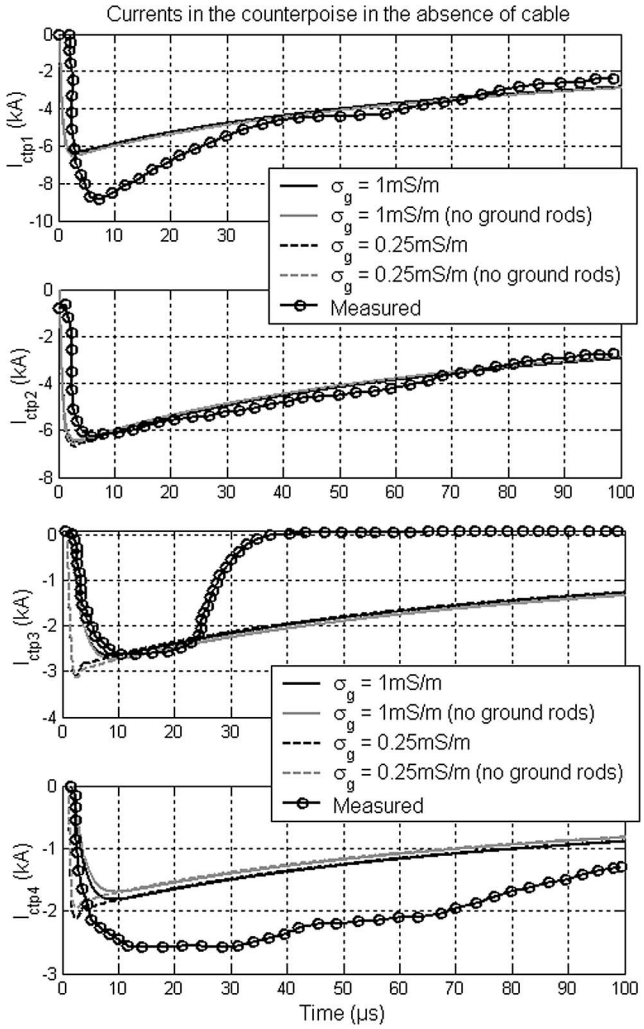

Fig. 5. Model-predicted counterpoise currents, $I_{\mathrm{ctp1}}, I_{\mathrm{ctp2}}, I_{\mathrm{ctp3}}$, and I_{ctp4}, in the absence of the cable with and without ground rods for two values of ground conductivity, 1 and 0.25 mS/m. Also shown are measured currents.

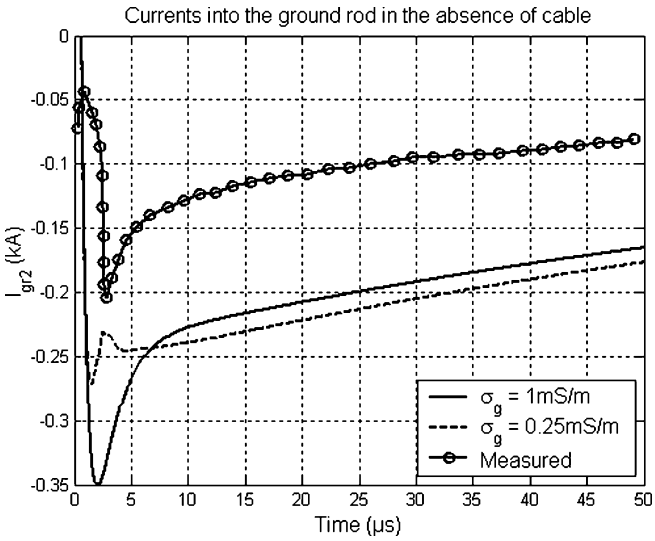

Fig. 6. Model-predicted currents into one of the ground rods, I_{gr2}, in the absence of the cable for two values of ground conductivity, 1 and 0.25 mS/m. Measured current is also shown.

ferent decaying portion of I_{ctp3}. Interestingly, measured I_{ctp3} exhibited a similar waveshape for other lightning flashes, although its width varied. The simulated and measured waveforms for I_{ctp4} seem to agree at early times, but a significant discrepancy is seen at late times. Since I_{ctp1} and I_{ctp4} measurement points are on the same side of the current injection point, it is expected that waveforms of I_{ctp1} and I_{ctp4} should have similar shapes with some difference in magnitude due to propagation losses. Reasons for different shapes of I_{ctp1} and I_{ctp4}, suggesting considerable dispersion, are presently unknown.

B. Counterpoise, Cable, and Ground Rod Currents—Two Conductors With Ground Return Analysis

Here, we will simulate a configuration with both the cable and counterpoise included using the equations presented in previous section. It is to be noted that the lightning current injection point is not equidistant from the terminations or ground rods. Hence, the time of arrival of possible reflections from the line discontinuities should be different. This is particularly important for the case of the cable for which the speed of current waves is faster than for the counterpoise.

Simulated currents in the counterpoise are shown in Fig. 7 for I_{ctp1} (first window), I_{ctp2} (second window), I_{ctp3} (third window), and I_{ctp4} (fourth window). The current I_{gr2} into the ground rod in the presence of cable is shown in Fig. 8. The simulated currents in the cable are shown in Fig. 9 for I_{c1} (first window), I_{c2} (second window), I_{c3} (third window), and I_{c4} (fourth window). It is observed that currents I_{ctp1} and I_{ctp2} in the counterpoise are not much different in terms of their magnitude from the case when the counterpoise alone was simulated (compare Figs. 5 and 7). There are some oscillations in the current waveforms for I_{ctp1} and I_{ctp2} due to the presence of the cable. Similar observations can be made for the current waveforms of I_{ctp3} and I_{ctp4} (compare the bottom two windows in Figs. 5 and 7). Specifically, computed magnitudes of I_{ctp4} in the presence of cable are about 35% higher as compared to the corresponding case with the cable absent.

As seen from comparison of Figs. 6 and 8, the presence of cable does not much affect the model-predicted currents in the ground rod. It appears that for the examined system configurations, ground rods do not contribute much to the dissipation of current in the ground.

It is to be acknowledged that the agreement between the simulated and measured cable currents is poor. For I_{c2} and I_{c3}, even the polarity is not reproduced correctly. Also, the magnitude of model-predicted I_{c4} is almost an order of magnitude larger than measured. The computed currents in the cable are, in general, oscillatory, perhaps due to the cable capacitance and/or together with the capacitance of the pipe, which dominates at higher frequencies the total mutual admittance between the cable and counterpoise. Similar oscillations were observed by Bejleri [2] who modeled the system using alternative transients program–electromagnetic transients program (ATP–EMTP) [9] software. However, no oscillations are seen in corresponding measured waveforms. Perhaps at higher frequencies, primarily during the current rise time, the modeled cable acts like a bare conductor,

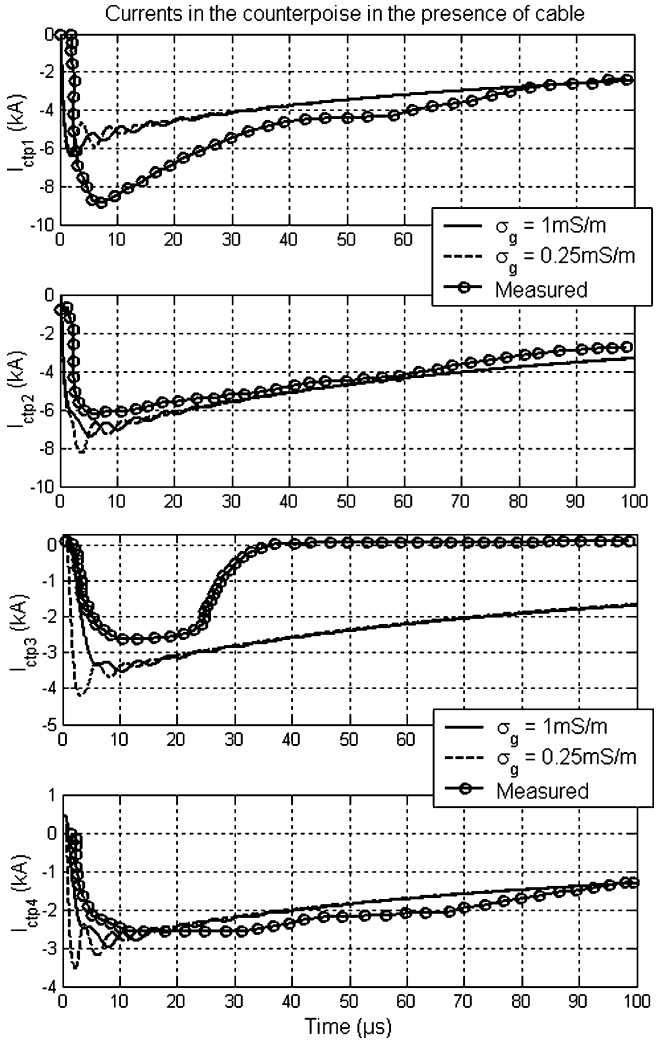

Fig. 7. Model-predicted counterpoise currents I_{ctp1}, I_{ctp2}, I_{ctp3}, and I_{ctp4} in the presence of cable for two values of ground conductivity, 1 and 0.25 mS/m. Also shown are measured currents.

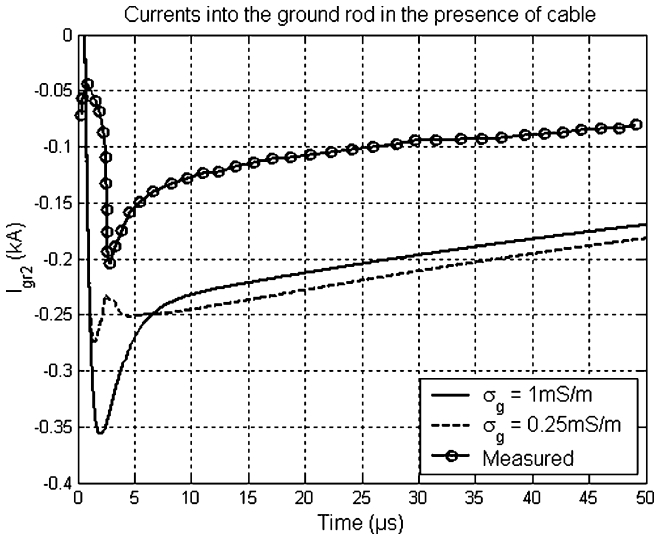

Fig. 8. Model-predicted currents into one of the ground rods, I_{gr2}, in the presence of the cable for two values of ground conductivity, 1 and 0.25 mS/m. Also shown is the measured current.

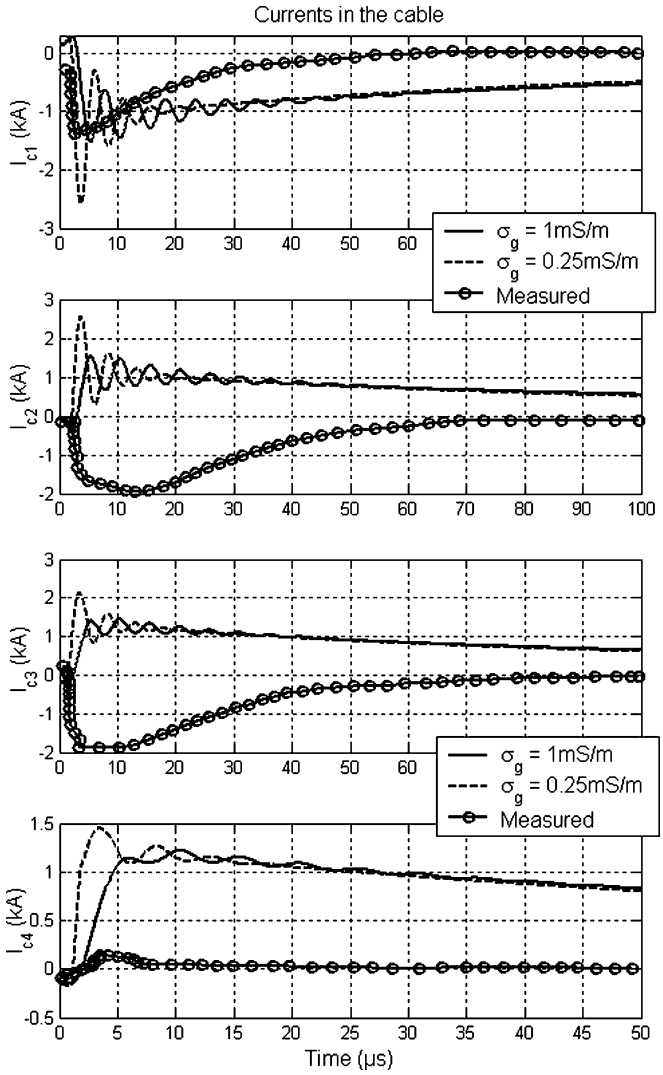

Fig. 9. Model-predicted cable currents I_{c1}, I_{c2}, I_{c3}, and I_{c4} for two values of ground conductivity, 1 and 0.25 mS/m. Also shown are the measured currents.

i.e., higher currents in the cable are observed when the ground conductivity is poor, and the higher the ground conductivity, the larger the oscillations in the current. Note that simulated cable currents I_{c1} and I_{c2} are in opposite directions in contrast with the counterpoise currents I_{ctp1} and I_{ctp2} (compare Figs. 7 and 9). We speculate that it could be due to asymmetry of the line relative to the lightning current injection point.

Bejleri *et al.* [1] have also measured the voltages between the cable and counterpoise at two points, V_1 and V_4, shown in Fig. 1. A comparison between the model-predicted and measured voltages is shown in Fig. 10. The polarity of V_4 is not correctly reproduced, and the waveshapes are very different (several microseconds durations predicted by the model versus submicrosecond-scale pulses observed).

The initial polarity of calculated voltage waveforms suggests that the counterpoise is at a higher potential than the cable. In principle, potentials should be higher for the counterpoise than for the cable since the currents in the cable are smaller as compared to those in the counterpoise. However, as expected, it is seen that the voltage between the cable and counterpoise is

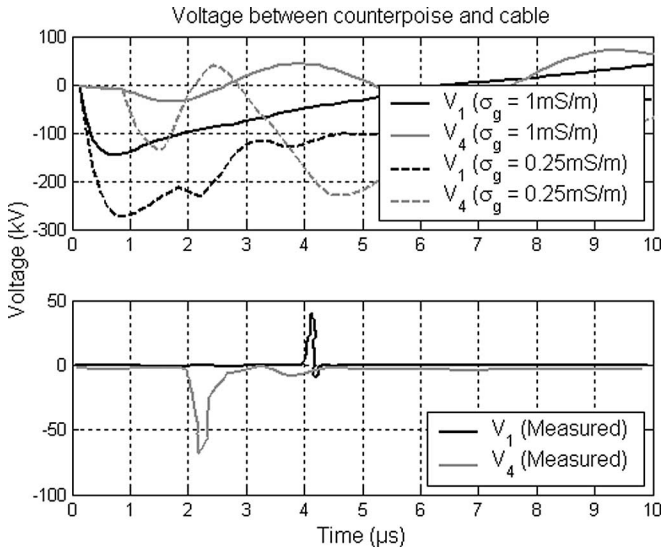

Fig. 10. Model-predicted voltage between counterpoise and cable, V_1 and V_4 (top window), for two values of ground conductivity, 1 and 0.25 mS/m, and the corresponding measured voltages (bottom window). The polarity of measured V_1 indicates that the cable was at a higher potential than the counterpoise, while for V_4 the counterpoise was at a higher potential than the cable.

higher for V_1 as compared to V_4 since V_1 is measured closer to the current injection point (see Fig. 1). It is also seen from the simulations that the voltage depends on ground conductivity, the poorer the ground conductivity, the larger the voltages. Note that the insulation strength of the cable is 5 kV, which is much lower than either measured of calculated voltage peaks. The measured voltages exhibit shapes indicative of insulation breakdown. On the other hand, no evidence of direct lightning current injection into the cable or flashover to the cable from the counterpoise was found [1]. It appears that the voltage between the counterpoise subjected to lightning current and the cable is reduced rapidly enough to save the cable insulation from significant damage. This is likely to be due to transient bonding (capacitive or resistive coupling or both) of the cable and counterpoise at early times.

VI. Discussion

In the TLM approach adopted here, we ignored the external electromagnetic fields that can additionally excite the system, since the lightning channel is very close to the system under study. Perhaps the entire system is nearly simultaneously excited. The exciting electromagnetic fields on the counterpoise and the cable should be similar to the ones on the surface of the ground. This is because the depth of either the cable or counterpoise is not sufficient to bring about significant field attenuation, because the ratio of fields at depth d and at the surface is close to unity, i.e., $E_d/E_{d=0} \approx e^{-\gamma_g d} \approx 1$ [10]. Note that for incorporating the field to wire coupling models, one needs to know the components of fields along the conductors, which is difficult in the current problem since the conductors are relatively short and form closed loop. There is also an uncertainty regarding the actual sources exciting the counterpoise, because the counterpoise is also carrying the injected current. It is not clear if the conventional way of distributing the sources corresponding to nearby

strikes, as done in [11] and [12], is suitable here or not. Some attempts to calculate lightning-induced voltages in loops located inside a building that was struck by lightning have been made by Metwally *et al.* [13]. The exciting fields due to currents in the lightning channel and building's down conductors were used for the calculations.

The measured peak currents in the counterpoise at I_{ctp1} and I_{ctp2} are about 9 and 6 kA, respectively; whereas, the currents in the cable I_{c1} and I_{c2} are about 1.5 and 2 kA, respectively (compare top two windows of Figs. 7 and 9). Assuming linearity in the coupling mechanism, we expect that the induced cable current I_{c1} should have been larger than I_{c2}. The simulated currents for I_{ctp1} and I_{ctp2} are about 6 and 8 kA, and the simulated cable currents I_{c1} and I_{c2} are both about 2 kA (although of opposite polarity). Note that the simulated waveshapes of I_{c2} and I_{c3} are almost identical even though they are at two different distances on the same side from the injection point. The measured currents I_{c2} and I_{c3} in the cable (although of opposite polarity) show a similar behavior. This is as expected because in the cable the attenuation of currents is much less as compared to that in the counterpoise. The attenuation factors for a counterpoise and a cable in the soil is given by

$$\alpha_{\mathrm{ctp}}\left(j\omega\right) = \mathrm{Re}\left[\sqrt{Z_g Y_g}\right] \tag{21}$$

$$\alpha_c\left(j\omega\right) = \mathrm{Re}\left[\sqrt{\left(j\omega L_i + Z_g\right)\left(\frac{j\omega C_i Y_g}{j\omega C_i + Y_g}\right)}\right] \tag{22}$$

which are obtained by taking the real parts of the propagation constants, respectively.

The velocities of the propagating waves along the counterpoise and cable in the soil are given respectively by

$$v_{\mathrm{ctp}}\left(\omega\right) = \frac{\omega}{\mathrm{Im}\left[\sqrt{Z_g Y_g}\right]} \tag{23}$$

$$v_c\left(\omega\right) = \frac{\omega}{\mathrm{Im}[\sqrt{\left(j\omega L_i + Z_g\right)\left(j\omega C_i Y_g/\left(j\omega C_i + Y_g\right)\right)}]} \tag{24}$$

which are obtained by taking the ratio of ω and the imaginary parts of the appropriate propagation constants.

In (21)–(24), Z_g and Y_g are the ground impedance and ground admittance, respectively, of either the counterpoise or the cable as the case may be. L_i and C_i are the inductance and capacitance, respectively, due to the insulation sheath thickness of the cable if the cable is in direct contact with the soil; else it is the combined inductance and capacitance for the case when the cable is in the pipe, as discussed earlier. Fig. 11 shows the ratio of attenuation constants $\alpha_{\mathrm{ctp}}/\alpha_c$ for the counterpoise–cable configuration under study and for two values of ground conductivity, 1 and 0.25 mS/m. It is clear that only at high frequencies, the ratio of attenuation constants is close to unity and perhaps the cable and counterpoise behave similarly. But, at lower frequencies, attenuation in the counterpoise is much larger than in that the cable. Current I_{c4} is different from I_{c3} because of the presence of load representing the current regulator.

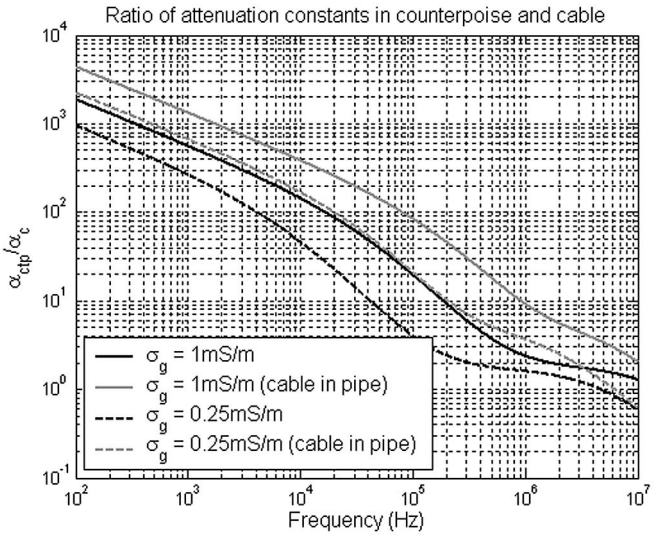

Fig. 11. Ratio of attenuation constants for the counterpoise and the cable (in direct contact with the soil or in the pipe) for two values of ground conductivity, 1 and 0.25 mS/m.

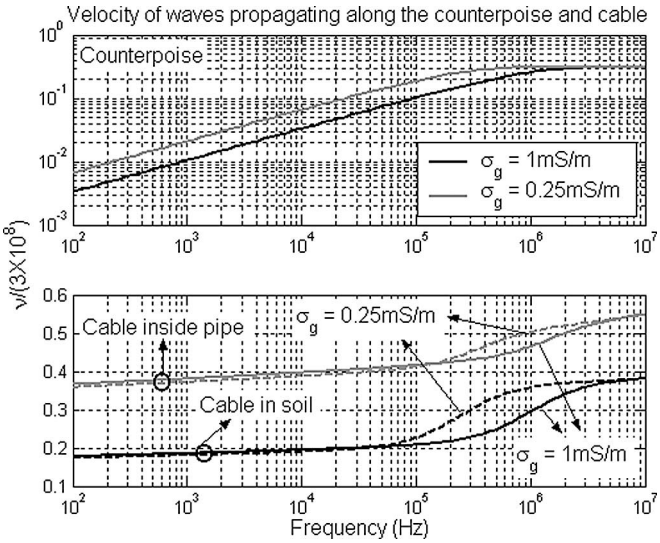

Fig. 12. Velocities of waves propagating along the counterpoise (upper window) and the cable either in direct contact with the soil or in the pipe (lower window) with respect to the speed of light in free space for two values of ground conductivity, 1 and 0.25 mS/m.

The velocities of the waves propagating along the counterpoise and cable with respect to the speed of light in free space are shown in Fig. 12. For the case when the cable is in direct contact with the soil, the velocity at high frequencies of the waves propagating is similar to that in the counterpoise. However, at lower frequencies, the velocities are much lower for the counterpoise than for the cable. When the cable is in the PVC pipe, the velocity for the cable is higher by about a factor of one and half than that for the case when the cable is in direct contact with the soil. This effect is observed at all frequencies.

It is likely that there was electrical breakdown between the cable and counterpoise and soil ionization around the counterpoise. Bejleri *et al.* [1] did not rule out such possibility. Measured voltage waveforms (see Fig. 10) appear to be

indicative of breakdown between the cable and the counterpoise somewhere in the system. It is not clear though where exactly in the system, the breakdown and soil ionization could have occurred. These nonlinear phenomena can significantly affect the current distributions along the counterpoise and cable. The aim of this research was to examine capabilities of a simple TLM. Numerical electromagnetic or hybrid methods (including nonlinear effects and electromagnetic coupling with the lightning channel) could be tried in a future investigation.

VII. Concluding Remarks

A test airport runway lighting system was subjected to direct lightning strikes and currents measured in different parts of the system were reported by Bejleri *et al.* [1]. In this paper, an attempt is made to model the lightning interaction of this system using the transmission line theory. The model-predicted currents in the counterpoise, ground rod, and the cable were compared with the measurements and a reasonable agreement was found for the currents along the counterpoise. Current in the counterpoise is not much influenced by the presence of the cable. Further, vertical ground rods connected to the counterpoise do not have significant influence on the current distribution along the counterpoise. It appears that the model is not suitable for predicting cable currents and voltages in the test system, presumably due to neglecting nonlinear phenomena in the soil and in cable's insulation and electromagnetic coupling with the lightning channel. Moreover, the rectangular loop formed by the cable-counterpoise system is not necessarily a uniform transmission line system. There are also many questionable assumptions regarding the system configuration (e.g., neglecting transformers and the resistive-inductive representation of the source). All these factors will be examined in more detail in a future study.

References

[1] M. Bejleri, V. A. Rakov, M. A. Uman, K. J. Rambo, C. T. Mata, and M. I. Fernandez, "Triggered lightning testing of an airport runway lighting system," *IEEE Trans. Electromagn. Compat.*, vol. 46, no. 1, pp. 96–101, Feb. 2004.

[2] M. Bejleri, "Triggered-lightning testing of an airport runway lighting system," M.Sc thesis, Univ. Florida, Gainesville, FL, 1999.

[3] L. M. Wedepohl and D. J. Wilcox, "Transient analysis of underground power transmission systems: System-model and wave propagation characteristics," *Proc. Inst. Elect. Eng.*, vol. 20, no. 2, pp. 253–260, 1973.

[4] E. D. Sunde, *Earth Conduction Effects in the Transmission Systems*. New York: Van Nostrand, 1949.

[5] F. M. Tesche, M. V. Ianoz, and T. Karlsson, *EMC Analysis Methods and Computational Models*. New York: Wiley, 1997.

[6] N. Theethayi, R. Thottappillil, M. Paolone, C. A. Nucci, and F. Rachidi, "External impedance and admittance of buried horizontal wires for transient studies using transmission line analysis," *IEEE Trans. Dielectr. Electr. Insul.*, vol. 14, no. 3, pp. 751–761, Jun. 2007.

[7] N. Theethayi, "Electromagnetic interference in distributed outdoor electrical systems, with an emphasis on lightning interaction with electrified railway network," Ph.D. thesis, Uppsala Univ., Sweden, 2005.

[8] E. F. Vance, *Coupling to Shielded Cables*. New York: Wiley, 1978.

[9] W. S. Meyer and T. Liu, "Alternative Transient Program (ATP) rule book, copyright 1987–1992 by Canadian/American EMTP user group."

[10] V. Cooray, "Underground electromagnetic fields generated by the return strokes of lightning flashes," *IEEE Trans. Electromagn. Compat.*, vol. 43, no. 1, pp. 75–84, Feb. 2001.

[11] J. D. Nordgard and C. L. Chen, "Lightning-induced transients on buried shielded transmission lines," *IEEE Trans. Electromagn. Compat.*, vol. 21, no. 3, pp. 171–181, Nov. 1979.

[12] E. Petrache, F. Rachidi, M. Paolone, C. A. Nucci, V. A. Rakov, and M. A. Uman, "Lightning induced disturbances in buried cables—Part I: Theory," *IEEE Trans. Electromagn. Compat.*, vol. 47, no. 3, pp. 498–508, Aug. 2005.

[13] I. A. Metwally, F. H. Heidler, and Z. Zischank, "Magnetic fields and loop voltages inside reduced and full-scale structures produced by direct lightning strikes," *IEEE Trans. Electromagn. Compat.*, vol. 48, no. 2, pp. 414–426, May 2006.

Nelson Theethayi (S'04–M'06) was born in India, in 1975. He received the B.E. degree in electrical and electronics (first class distinction) from the University of Mysore, Mysore, India, in 1996, the M.Sc. (Engineering) degree in high-voltage engineering from the Indian Institute of Science, Bangalore, in 2001, and the Ph.D. degree in electricity with specialization in electrical transients and discharges from Uppsala University, Uppsala, Sweden, in 2005.

He is currently a Researcher at the Electromagnetic Compatibility (EMC) Group of the Division for Electricity, Uppsala University. His current research interests include EMC, high-voltage engineering, electrical power systems, modeling and experimental investigation of lightning phenomena and lightning interaction, and analysis and design of lightning-protection systems for power, railway, and communication systems.

Dr. Theethayi is a member of Subcommittee "Lightning" of the Technical Committee TC5 of the IEEE EMC Society, IEEE Dielectrics and Electrical Insulation Society, IEEE Power Engineering Society, and IEEE Industry Applications Society.

Vladimir A. Rakov (SM'96–F'03) received the M.S. and Ph.D. degrees in electrical engineering from Tomsk Polytechnical University (Tomsk Polytechnic), Tomsk, Russia, in 1977 and 1983, respectively.

He is currently a Professor in the Department of Electrical and Computer Engineering, University of Florida, Gainesville, and the Co-Director of the International Center for Lightning Research and Testing, Starke, FL. From 1977 to 1979, he was an Assistant Professor of Electrical Engineering at Tomsk Polytechnic. During 1978, he was with the High-Voltage Research Institute, a division of Tomsk Polytechnic, where, from 1984 to 1994, he was the Director of the Lightning Research Laboratory. He is the author or coauthor of more than 140 papers published in international journals and is a coauthor of a book. He holds more than 30 patents.

Dr. Rakov is a Fellow of the American Meteorological Society and the Institution of Engineering and Technology. He is a member of the American Geophysical Union, the Society of Automotive Engineers (now SAE International), and the American Society for Engineering Education. He is serving as the Chairman of the Technical Committee on Lightning of the biennial International Zurich Symposium on Electromagnetic Compatibility. He was the Chairman of the American Geophysical Union Committee on Atmospheric and Space Electricity.

Rajeev Thottappillil (S'88–M'92–SM'06) was born in India in 1958. He received the B.Sc. degree from the University of Calicut, Kerala, India, in 1981, and the M.S. and Ph.D. degrees from the University of Florida, Gainesville, in 1989 and 1992, respectively, all in electrical engineering.

Since 1996, he has been with Uppsala University, Uppsala, Sweden, where he was earlier an Associate Professor, and currently, a Full Professor in the subject area of electricity with special emphasis on transients and discharges at the Division for Electricity, Department of Engineering Sciences. His current research interests include lightning phenomenon, electromagnetic interference, and electromagnetic field theory. He is the author or coauthor of more than 150 scientific papers, about 60 of them are in refereed journals, and five book chapters.

Prof. Thottappillil is the Chairman of the European Union (EU) project COST action P18 "Physics of Lightning Flash and its Effects." He is a member of the SC 77C of SEK, International Electrotechnical Commission (IEC) on High-Power Transients, and the Subcommittee "Lightning" of the Technical Committee TC5 of the IEEE Electromagnetic Compatibility Society.